ISSN: 0974-5823 Vol. 7 No. 1 January, 2022

International Journal of Mechanical Engineering

Enhancement physical properties of Cu-doped α-Fe_2O_3 thin films deposited by Chemical spray pyrolysis

Oday Ali Chichan
Department of Physics, College of Education for Pure Sciences, University of Babylon, Iraq.

Shaymaa Hussein Nowfal
Department of Biomedical Engineering, College of Engineering University of Warith Al-Anbiyaa Karbala 56001, Iraq.

Huda Nagem Abd
[3]Ministry of Education, Vocational Education, Baghdad, Iraq.

Khalid Haneen Abass
Department of Physics, College of Education for Pure Sciences, University of Babylon, Iraq.

Nadir Fadhil Habubi
Department of Physics, College of Education, Mustansiriyah University, Baghdad, Iraq.

Sami Salman Chiad*
Department of Physics, College of Education, Mustansiriyah University, Baghdad, Iraq.

Abstract

Hematite (α-Fe_2O_3) doped with copper (Cu) at two various concentrations (2% and 4%) were synthesized through Chemical spray pyrolysis (CSP) method. XRD results approve that all the prepared nano-crystals comprise hematite phase. The crystal size increases from 12.39 nm to 14.56 nm with the increase in Cu content. AFM images assure the nanostructured of the intended films with an average particle size ranging 50.13 to 57.93 nm. from UV–Vis measurements it can be verified that the increase in crystallite size is associated with a decrease in bangap. Sample with 4% Cu-doped α -Fe_2O_3 exhibit lower energy gap of (2.46) eV as compared to the un-doped α -Fe2O3 which was (2.38) eV.

Keyword: CSP, α-Fe_2O_3 , Fe_2O_3:Cu, XRD, AFM.

Introduction

FeO, Fe_3O_4, α-Fe_2O_3, and γ-Fe_2O_3 are the most common iron oxide [1, 2]. Based on preparation methods and circumstances, different stoichiometry and crystalline can be obtained. However, (α-Fe_2O_3) is ultimately stable phase [3,4] that characterized by a bandgap of 2.2 eV. (α-Fe_2O_3) has gained a lot of interest because of its valuable physical and chemical characteristics [5- 8]. To enhance the properties of α-Fe2O3, some researchers groups used doping with various elements, One approach of that is donor doping, such Ti^{4+}, Sn^{4+}, Si^{4+} [13], etc. while the second is acceptor doping, such Mg^{2+} [14], Zn^{2+} [15], Cu^{2+} [16, 17], Ag^{+} [18], etc. The applications of Iron oxide are not limited to photoelectron-chemical water splitting [19-22] but also extended to lithium-ion batteries [23,47-67], sensors [24], [25], magnetism and medical applications[26], etc. Different techniques used to deposition Iron Oxide such as spin coating [27], DC magnetron sputtering [28], electrochemical depositions [29], hydrothermal [30] and spray pyrolysis [31], etc. In this paper, we study the modification of some physical properties of Fe_2O_3 nano-crystalline Cu2+. Since, the radius of Cu2+ is larger than that of Fe3+, doping with Cu may differ from that of other ions.

Experimental

Undoped Fe_2O_3 and Fe_2O_3:Cu thin films were deposited on glass bases by (CPS) method. A lab made glass atomizer was exploited for spraying the chemical solution at a temperature of 450°C. 0.1 M of both $FeCl_3$ and $CuCl_2$. Spraying rate was 0.2 mL /spray, base to spout was 30 cm, spraying time was 8 s, stopping after each spray was 2 min, and N_2 fixed at a pressure of 10^5 Pa as conveyor gas. Film thickness is measured by gravimetric method. The grown films have a thickness of 350 ± 25 nm. Structural parameters were evaluated by XRD after that AFM were operated to define their structure and morphology, transmittance spectra are obtained utilizing UV-visible double spectrophotometer.

Results and discussion

The key peaks are from the diffraction intensity of α-Fe_2O_3 and doping Fe_2O_3: Cu layer are shown in Figure 1. Both undoped and Cu doped samples reveal α phase of Fe_2O_3 (JCPDS card No. 40-1139) after doping. The peaks acting at a 2θ range of 24.60°, 30.18°, 50.35° and 62.76° can be attributed to the 017, 110, 127 and 220 crystalline structures corresponding to α-Fe_2O_3 thin films. There are no characteristic peaks of CuO or CuO_2 in the Cu doped film. However, the position of characteristic peaks shifts slowly after Cu doping, this indicates Cu will not disturb the lattice strongly and structure of α-Fe_2O_3 remains unchanged. Furthermore, increasing Cu concentration causes the strength of (110) peak to steadily grow while the half height breadth of the peak decreases. The rise can be attributed to the fact that Cu serves as nucleation sites for crystalline grain development.. This corresponds to a decrease in the half width of the diffraction peaks, suggesting an increase in grain size as compared to the pure sample. When Cu^{2+} ions are merged into α-Fe_2O_3, the lattice parameters might be slightly changed, causing α-Fe_2O_3 peaks shift [32].

The crystallite size "*D*" is estimated from Scherer's equation [33].

$$D = \frac{k\lambda}{\beta cos\theta} \qquad -----1$$

Here k represents the shape factor which is equal to 0.9, λ is the wavelength of x-ray, β is FWHM, and θ is the Bragg angle. To determine *D* of the intended films, the (110) plane was chosen, it is found to be ranged between 12.39 nm and 14.56 nm. Table 1 shows that *D* of the intended films. There is a clear enhancing in the crystal structure in the doped samples as the copper content is increased. The oxygen vacancies in Fe_2O_3:Cu spreads slightly with increases concentration doping with Cu and this lead to change in crystal structural [34]. Dislocation density (δ)) of Fe_2O_3 nanostructure is considered empploying the following equation (2): [35, 36]:

$$\delta = \frac{1}{D^2} \qquad -----2$$

Micro strain (ε) of the Fe_2O_3 nanostructure was calculated using the following equation (3) [35, 36]:

$$\varepsilon = \frac{\beta cos\theta}{4} \qquad -----3$$

Fig.2 shows the crystallite size, FWHM, strain and δ with dopant. *D* increase and ε and the δ decrease caused by the doping of Cu create more oxygen vacancies in order to neutralize the charge in Fe_2O_3 lattice [34]. The increase in grain size resulting in the reduction of strain and dislocation density leads to tensile strain, when Cu^{2+} ions incorporated into interstitial sites in the α-Fe_2O_3 lattice [37]. The structural parameters are calculated for the preferred (110) peak and given in Table 1.

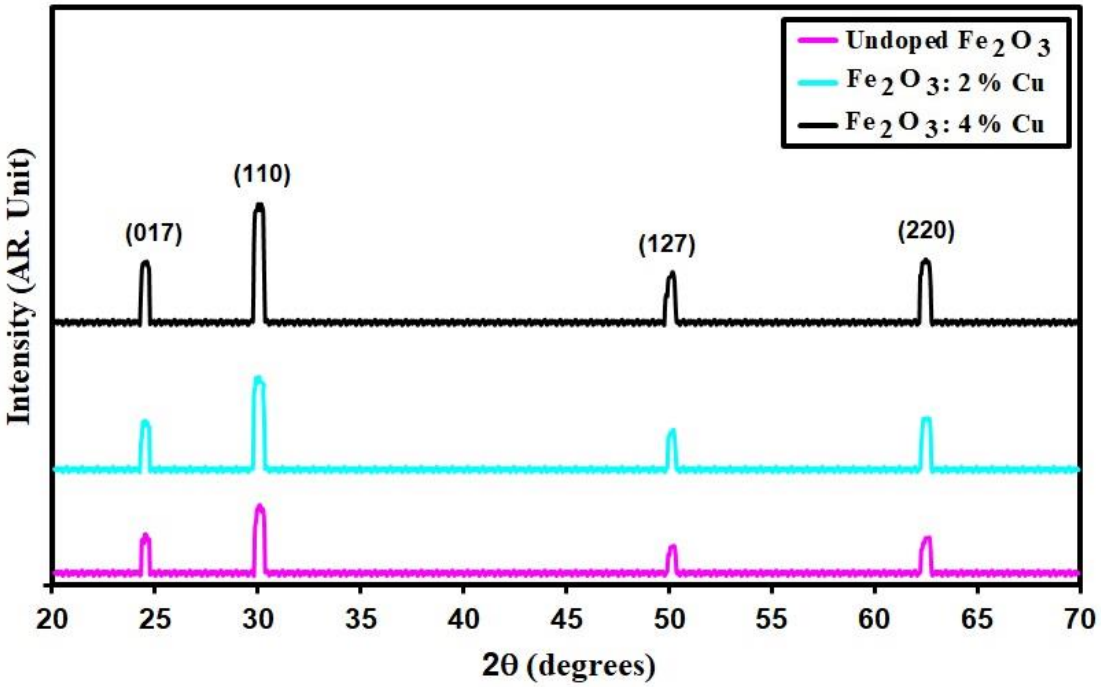

Fig. 2. XRD patterns of grown films.

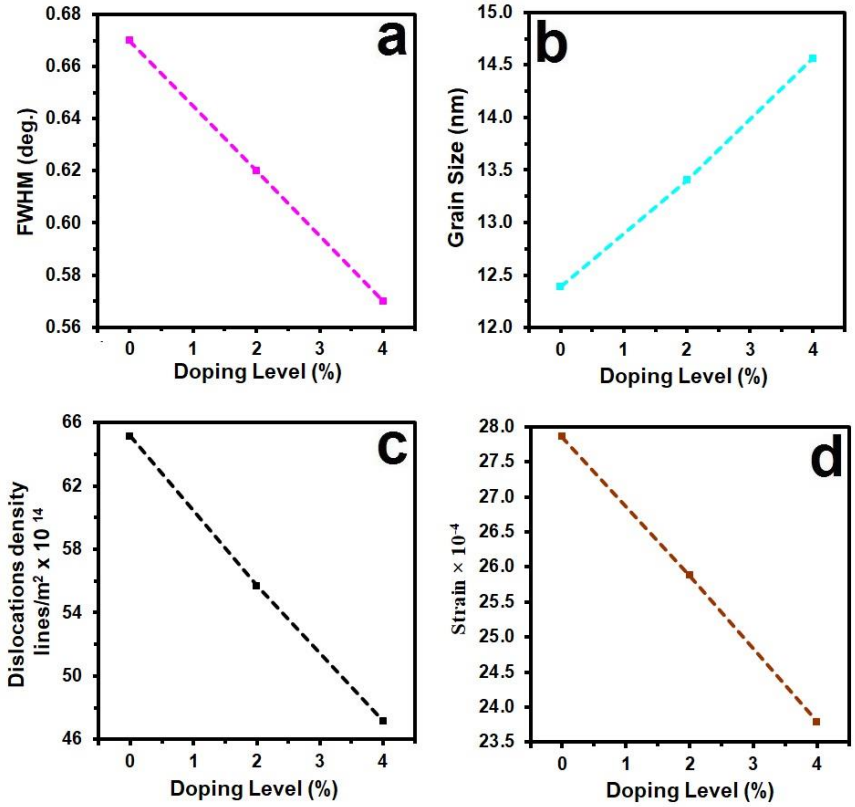

Fig. 2. X-ray parameter grown films.

Table 1. structure parameters of grown films.

Specimen	(hkl) Plane	2 □ (º)	FWHM (º)	Optical bandgap (eV)	Grain size (nm)	Dislocations density (× 10^{14}) (lines/m^2)	Strain (× 10^{-4})
Undoped Fe_2O_3	110	30.18	0.67	2.46	12.39	65.14	27.86
Fe_2O_3: 2% Cu	110	30.12	0.62	2.42	13.40	55.69	25.88
Fe_2O_3: 4% Cu	110	30.08	0.57	2.38	14.56	47.17	23.79

Atomic force microscopy analysis

Fig. 3 shows three dimensional (3D) AFM images and particles size distribution of the α-Fe_2O_3 and doping in Cu nanostructure thin films scanned over a surface area of 78nm × 78nm. The AFM image of α-Fe_2O_3 shows the influence of the doping on the crystalline growth. One can easily have noticed the increase in size distribution of grains after doping with Cu. The statistical roughness R_a analysis of α-Fe_2O_3 shows that the obtained roughness average is 6.36nm, and decreases with increase doping with Cu. The average particles size P_{av} and root mean square roughness R_{rms} are same behavior of roughness in undoing and doping. The results show that sharpness of the grains is dominated of surface. The size distribution of nanoparticles is shown in Fig. 3. All The resulting AFM images are demonstrate that the films are summarized in table 2.

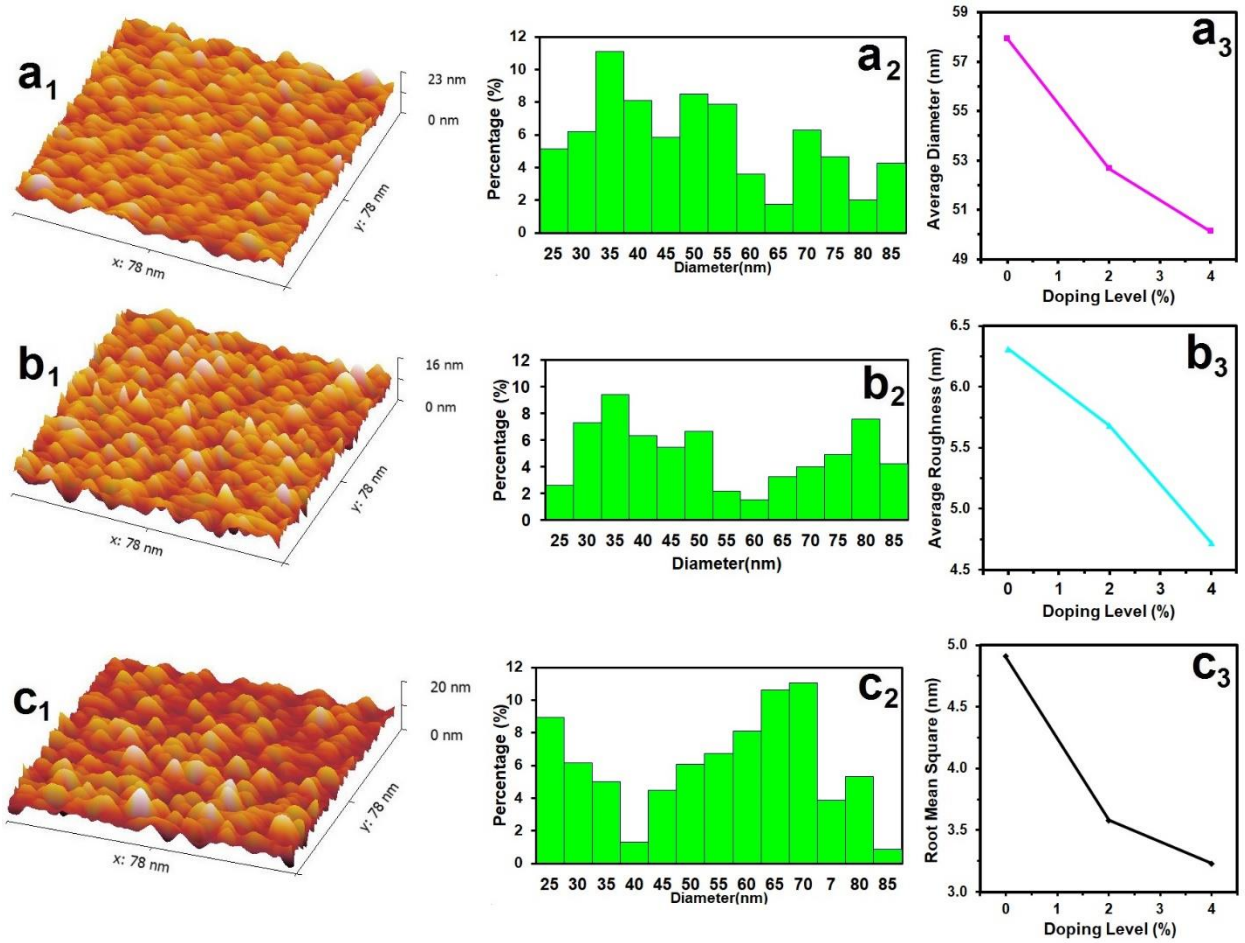

Fig.3. AFM of pure and Cu-doped Fe_2O_3 films.

Table 2. AFM parameter measurement of pure and Cu-doped Fe_2O_3 films.

Samples	P_{av} nm	R_a (nm)	R_{rms} (nm)
Undoped Fe_2O_3	57.93	6.31	4.91
Fe_2O_3: 2% Cu	53.68	5.68	3.58
Fe_2O_3: 4% Cu	50.13	4.72	3.23

Optical Properties

Fig. (4), offers the transmittance T of the intended films. The results assure the dependence of T on Cu content. T in the visible area is found to be more than 90% and decreases with increase of doping due to increasing of the number of atoms and then the number of collision leading to the increase of absorbance. This finding is consistent with other published research. [38].

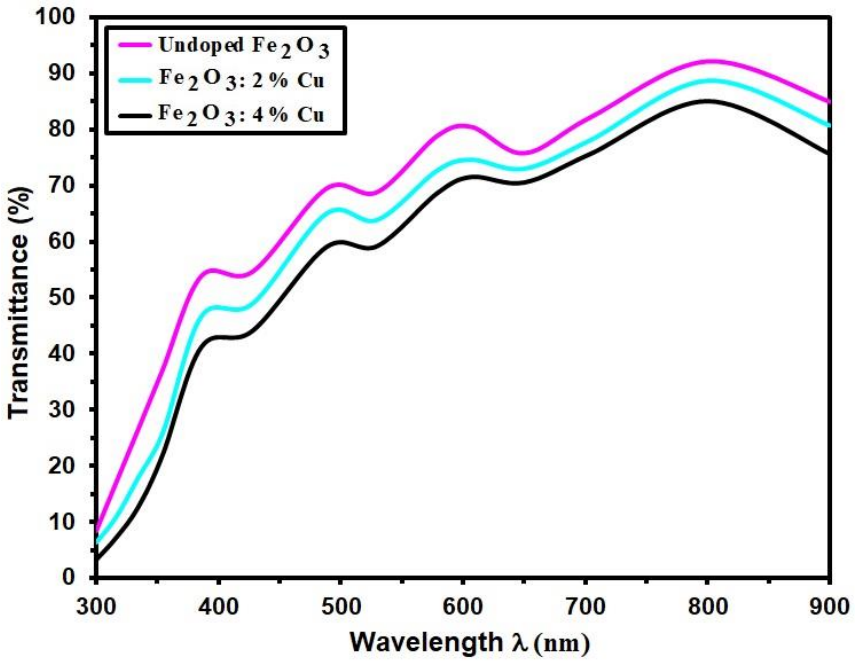

Fig. 4. Transmittance and b. α of pure and Fe_2O_3:Cu films with different dopant.

The absorption coefficient, α, was calculated from equation 4 [39] based on transmission values (T) and film thickness (d)

$$\alpha = \frac{1}{\frac{lnT}{d}} \quad -----4$$

Fig 5 displays the variation of α upon the incident wavelength at different Cu doping. The absorption coefficient has high values in order of 10^5 cm^{-1} for all films, also its value increased slightly with the increase of Cu doping concentration.

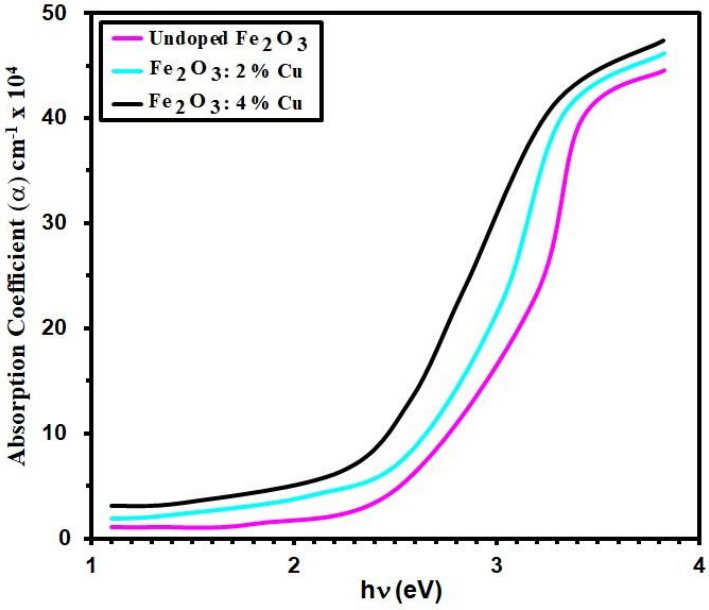

Fig. 5. α of grown films.

The optical band gap of Fe_2O_3 can be estimated from equation (5) [41,42]:

$$(\alpha h\nu) = A\left(h\nu - E_g\right)^n \quad -----5$$

where A is a constant and n = 1/2 and 2 for direct transitions. plots are offered in Figure 6. As Fe_2O_3:Cu is a direct transition semiconductor. The obtained band gap values of the direct transitions for the pure and Fe2O3: Cu films are in the range (2.46-2.38) eV for the films obtained at 450 oC substrate temperature. The obtained band gaps values of the direct transitions for the Fe_2O_3 films are in a good agreement with the Ref. [40]. This decrease in E_g with the increase of doping is assigned to the increase in crystallite size [43].

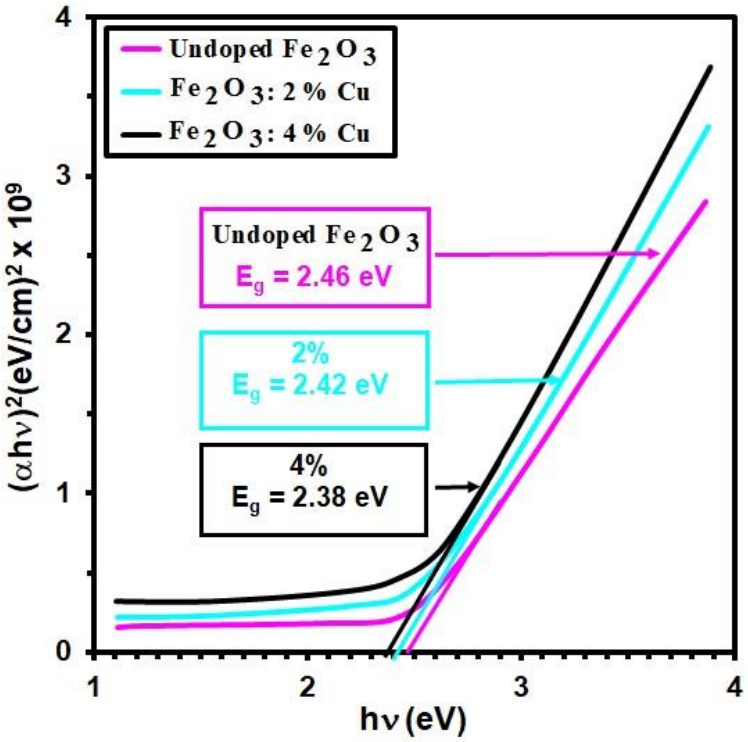

Fig.6. α of pure and Fe_2O_3:Cu films with different dopant.

The extinction coefficient (k) can be calculated using following equations [44]:

$$k = \frac{\alpha\lambda}{4\pi} \quad -----6$$

Fig. (7) shows k values of pure and Fe2O3:Cu thin films measured. k values increases slightly with the increase of λ and decreases sharply at λ=550 nm, and their values increase also with Cu doping.

The measurement of refractive index (n) is obtaind according to reflectance R values from the relation (7) [45]:

$$R = \frac{(n-1)^2}{(n+1)^2} \quad -----7$$

Fig. (8) shows the refractive index, there is a clear increase in (n) values by increasing the Cu doping content. This result could be due to the replacement of Cu by Fe_2O_3. Therefore, the ion refraction of Cu is higher than that of Fe which explains the increasing of (n) values by increasing Cu content. This behavior may be connected to the polarization of thin film as n values depend on material polarization.. Also (n) values increases with increase doping due to higher packing density [46].

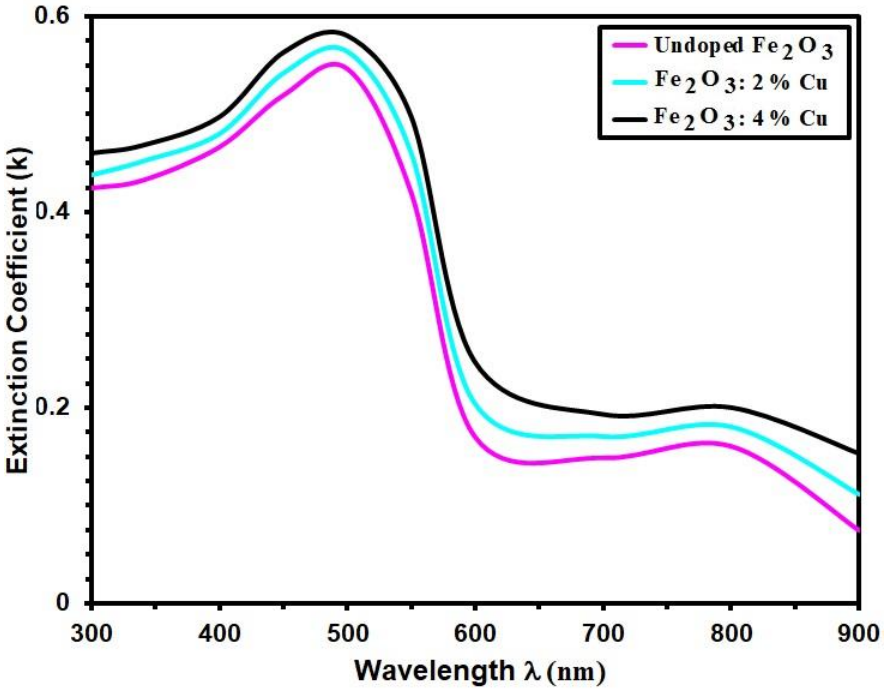

Fig. 7. k of pure and Fe_2O_3:Cu films with different dopant.

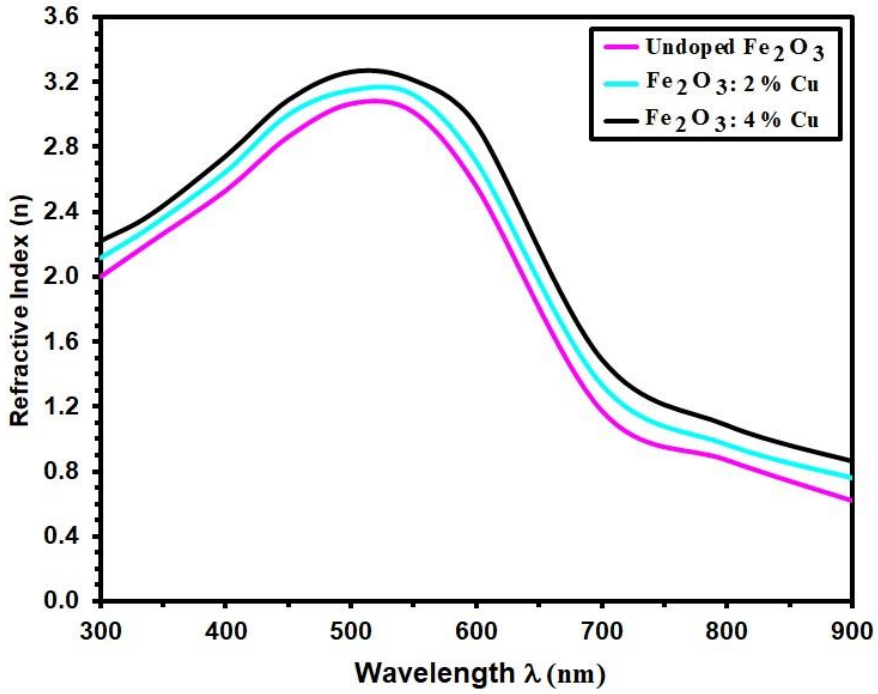

Fig. 8. *n* of pure and Fe_2O_3:Cu films with different dopant.

Conclusion

Nanocrystalline pure and Cu-doped α-Fe_2O_3 was successfully prepared by CSP. The XRD studies show that the both pure and Cu doped films demonstrate α phase of Fe_2O_3 thin films and the intensity of (110) direction is increased with the increase doping concentration. The average crystallite sizes derived from XRD data were between 12.39 nm and 14.56 nm. The AFM result of α-Fe_2O_3 shows uniform distribution for particles and the average roughness is 6.31 nm, and decreases with increase doping with Cu, the average particles size and root mean square roughness are same behavior. The transmission in visible area was more than 90%. The band gap decreased with the increase of doping.

Acknowledgments

This paper was supported by Mustansiriyah University (www.uomustansiriyah.edu.iq) and Alnukhba University College

References

[1] M.F. Al-Kuhaili, M. Saleem, S.M.A. Durrani, J. Alloy. Compd. 521, 178 (2012).
[2] H. Mansour, H. Letifi, R. Bargougui, S. De Almeida-Didry, B. Negulescu, C.A. Lambert, A. Gadri, S. Ammar, Appl. Phys. A.123, 787 (2017).
[3] A.A. Yadav, J. Mater. Sci.: Mater. Electron. 27, 12876–12883(2016).
[4] Z. Hubička, Š Kment, J. Olejníček, M. Čada, T. Kubart, M. Brunclíková, P. Kšírová, P. Adámek, Z. Remeš, Thin Solid Films 549,184 (2013).
[5] Q. Wei, Z. Li, Z. Zhang, Q. Zhou, " Facile Synthesis of α-Fe_2O_3Nanostructured Films with Controlled Morphology," Materials Transactions 50, 1351-1354(2009). [6] B. Issa, I. M. Obaidat, B. A. Albiss, Y. Haik, International journal of molecular sciences 14(11), 21266 (2013).
[7] K. Woo, J. Hong, S. Choi, H.-W. Lee, J.-P. Ahn, C. S. Kim, S. W. Lee, Chemistry of Materials 16 (14), 2814 (2004).
[8] S. Laurent, D. Forge, M. Port, A. Roch, C. Robic, L. Vander Elst, R. N. Muller,
Chemical reviews 108(6), 2064 (2008).
[9] R. Todorovska, S. Groudeva-Zotova, D. Todorovsky, Materials Letters 56(5), 770 (2002).
[10] S. Kulkarni, C. Lokhande, Materials chemistry and physics 82(1), 151 (2003). [11] A. A. Akl, Applied Surface Science 221(1), 319 (2004).
[12] A. Ali, M. Z. Hira Zafar, I. ul Haq, A. R. Phull, J. S. Ali, A. Hussain, Nanotechnology, Science and Applications 9, 49 (2016).
[13] A. Kay, I. Cesar, M. Gratzel, J. Am. Chem. Soc., 128, 15714-15721(2006).
[14] Y. Lin, Y. Xu, M.T. Mayer, Z.I. Simpson, G. McMahon, S. Zhou, D. Wang, J. Am. Chem. Soc., 134, 5508-5511(2012).
[15] W.B. Ingler, J.P. Baltrus, S.U.M. Khan, J. Am. Chem. Soc., 126, 10238-10239(2004).
[16] V.R. Satsangi, S. Kumari, A.P. Singh, R. Shrivastav, S. Dass, Int. J. Hydrogen Energ., 33, 312-318(2008).
[17] W.B. Ingler, S.U.M. Khan, Int. J. Hydrogen Energ., 30 (2005) 821-827.
[18] A. Watanabe, H. Kozuka, J. Phys. Chem. B, 107 (2003) 12713-12720.
[19] W. B. Ingler Jr. and S. U. M. Khan, Int. J. Hydrogen Energy 30, 821-827(2005).
[20] C. Leygraf, M. Hendewerk and G. Somorjai, J. Solid. State. Chem. 48, 357-367(1983).
[21] Y. Lin, Y. Xu, M. T. Mayar, Z. I. Simpson, G. McMahon, S. Zhou, D. Wang J. Am. Chem.Soc. 134, 5508-5511(2012).
[22] E. L. Tsege, T. S. Atabaev, M. A. Hossain, D. Lee, H. K. Kim, and Y. H. Hwang, "Cu-doped flower-like hematite nanostructures for efficient water splitting applications," J. Phys. Chem. Solids, vol. 98, pp. 283–289, 2016.
[23] B. Lucas-granados, R. Sánchez-tovar, R. M. Fernández-domene, and J. García-antón, "Applied Surface Science Controlled hydrodynamic conditions on the formation of iron oxide nanostructures synthesized by electrochemical anodization : Effect of the electrode rotation speed," Appl. Surf. Sci., vol. 392, pp. 503– 513, (2017).
[24] M. Orlandi et al., "On the effect of Sn-doping in hematite anodes for oxygen evolution," Electrochim. Acta, vol. 214, pp. 345–353(2016).
[25] M. Balogun et al., "High power density nitridated hematite (α- Fe2O3) nanorods as anode for high-performance flexible lithium ion batteries," J. Power Sources, vol. 308, pp. 7–17(2016).
[26] N. Pariona, K. I. Camacho-Aguilar, R. Ramos-González, A. I. Martinez, M. Herrera-Trejo, and E. Baggio-Saitovitch, "Magnetic and structural properties of ferrihydrite/hematite nanocomposites," J. Magn. Magn. Mater., vol. 406, pp. 221–227(2016).
[27] F. L. Souza, K. P. Lopes, P. A. P. Nascente, and E. R. Leite, "Nanostructured hematite thin films produced by spin-coating deposition solution: Application in water splitting," Sol. Energy Mater. Sol. Cells, vol. 93, no. 3, pp. 362–368(2009).
[28] M. C. Huang, T. Wang, C. C. Wu, W. S. Chang, J. C. Lin, and T. H. Yen, "The optical, structural and photoelectrochemical characteristics of porous hematite hollow spheres prepared by DC magnetron sputtering process via polystyrene spheres template," Ceram. Int., vol. 40, no. 7 PART B, pp. 10537–10544(2014).
[29] Q. Meng, Z. Wang, X. Chai, Z. Weng, R. Ding, and L. Dong, "Fabrication of hematite (α-Fe2O3) nanoparticles using electrochemical deposition," Appl. Surf. Sci.,vol.368, pp.303–308(2016).
[30] R. Rajendran, Z. Yaakob, M. Pudukudy, M. S. A. Rahaman, and K. Sopian, "Photoelectrochemical water splitting performance of vertically aligned hematite nanoflakes deposited on FTO by a hydrothermal method," J. Alloys Compd., vol. 608, pp.207–212(2014).
[31] Raid A.Ismail, Yassen Najim and Mohammad O. Dawood, " Spray Pyrolysis Deposition of α -Fe_2O_3 Thin Film," e-J. Surf. Sci. Nanotech. Vol. 6, 96-98(2008). [32] Shannon, R. D. Revised effective ionic radii and systematic studies of interatomic distances in halides and chalcogenides. Acta Cryst. 32, 751−767(976). [33] P. Klug, L.E. Alexander, X-Ray Diffraction Procedures: For Polycrystalline andAmor phous Materials, Wiley.32, 992-999(1974).
[34] Jiliang Zhang, Vincent Wing-hei Lau, Chang-Zhong Liao, Kam Wa Wong, Gi-Hyeok Lee, Feng Zou, Chung-Kai Chang, Hwo-Shuenn Sheu, and Yong-Mook Kang, " Controlling the Valence State of Cu Dopant in α -Fe_2O_3 Anodes: Effects on Crystal Structure

and the Conversion Reactions with Alkali Ions," Chem. Mater.,31,1268−1279(2019). [35]
S.T.Rattanachan, P.Krongarrom and T.Fangsuwannarak; American Journal of Applied Sciences, 10, 1427-1438 (2013).
[36] A. A. Akl and H. Howari, Journal of Physics and Chemistry of Solids 70, 1337 (2009).
[37] H.P. Shivaraju, G. Midhun, Anil Kumar KM, Pallavi S, Pallavi N, BehzadS.
Degradation of selected industrial dyes using Mg-doped TiO_2polyscales under
natural sun light as an alternative driving energy," J. Applied Water Science. 7
(2017) 3937–3948.
[38] S. Sivakumar, D. Anusuya, C. P Khatiwada, J. Sivasubramanian, A. Venkatesan and P. Soundhirarajan, " Characterizations of diverse mole of pure and Ni-doped α-Fe_2O_3 synthesized nanoparticles through chemical precipitation route," Spectrochimica Acta Part A: Molecular and Biomolecular Spectroscopy. 128, 69-75(2014).
[39] G. Hirankumar, Thermal, electrical and optical studies on poly (vinyl alcohol) based polymer electrolytes, in print.
[40] F. L. Souza, K. P. Lopes, P. A. P. Nascente, E. R. Leite, Solar Energy Mat. and Solar Cells 93 (2009) 362(2009).
[41] R. Branek, H. Kisch, Tuning the optical and photoelectrochemical properties of surfacemodified TiO2, Photochemical and Photobiological Sciences. 7, 40-48(2008).
[42] 50. F. Urbach, Phys. Rev. 92, 1324 (1953).
[43] M. F.A. Alias , R.M. Aljarrah , H. KH. Al-Lamy and K. A.W. Adem, "
Investigation the Effect of Thickness on the Structural and Optical Properties of Nano ZnO Films Prepared by d.c Magnetron Sputtering," J. I.J.A.I.E.M.,2 PP.198-
203(2013).
[44] P. E Agbo, M. N. Nnabuchi , Chalcogenide Letters 8, 273 (2011).
[45] Simmons, J., Potter, K.S.: Optical Materials, 1st edn. Academic Press, New York (1999).
[46] Y. A. AL Shaabani, " Studying Some Physical Properties Of $Zn_{2x}Cu_{1-x}In_{1-x}S_2$ thin Films Prepared by Chemical Spray Pyrolysis," Applied Sciences University of Technology,(2009).
[47] JALIL, A. T., DILFY, S. H., KAREVSKIY, A., & NAJAH, N. (2020). Viral Hepatitis in Dhi-Qar Province: Demographics and Hematological Characteristics of Patients. *International Journal of Pharmaceutical Research*, *12*(1). https://doi.org/10.31838/ijpr/2020.12.01.326
[48] Dilfy, S. H., Hanawi, M. J., Al-bideri, A. W., & Jalil, A. T. (2020). Determination of Chemical Composition of Cultivated Mushrooms in Iraq with Spectrophotometrically and High Performance Liquid Chromatographic. *Journal of Green Engineering*, *10*, 6200-6216.
[49] Jalil, A. T., Al-Khafaji, A. H. D., Karevskiy, A., Dilfy, S. H., & Hanan, Z. K. (2021). Polymerase chain reaction technique for molecular detection of HPV16 infections among women with cervical cancer in Dhi-Qar Province. *Materials Today: Proceedings*. https://doi.org/10.1016/j.matpr.2021.05.211
[50] Jalil, A. T., Kadhum, W. R., Khan, M. U. F., Karevskiy, A., Hanan, Z. K., Suksatan, W., ... & Abdullah, M. M. (2021). Cancer stages and demographical study of HPV16 in gene L2 isolated from cervical cancer in Dhi-Qar province, Iraq. *Applied Nanoscience*, 1-7. https://doi.org/10.1007/s13204-021-01947-9
[51] Widjaja, G., Jalil, A. T., Rahman, H. S., Abdelbasset, W. K., Bokov, D. O., Suksatan, W., ... & Ahmadi, M. (2021). Humoral Immune mechanisms involved in protective and pathological immunity during COVID-19. *Human Immunology*. https://doi.org/10.1016/j.humimm.2021.06.011
[52] Moghadasi, S., Elveny, M., Rahman, H. S., Suksatan, W., Jalil, A. T., Abdelbasset, W. K., ... & Jarahian, M. (2021). A paradigm shift in cell-free approach: the emerging role of MSCs-derived exosomes in regenerative medicine. *Journal of Translational Medicine*, *19*(1), 1-21. https://doi.org/10.1186/s12967-021-02980-6
[53] Hanan, Z. K., Saleh, M. B., Mezal, E. H., & Jalil, A. T. (2021). Detection of human genetic variation in VAC14 gene by ARMA-PCR technique and relation with typhoid fever infection in patients with gallbladder diseases in Thi-Qar province/Iraq. *Materials Today: Proceedings*. https://doi.org/10.1016/j.matpr.2021.05.236
[54] Saleh, M. M., Jalil, A. T., Abdulkereem, R. A., & Suleiman, A. A. Evaluation of Immunoglobulins, CD4/CD8 T Lymphocyte Ratio and Interleukin-6 in COVID-19 Patients. *TURKISH JOURNAL of IMMUNOLOGY*, *8*(3), 129-134. https://doi.org/10.25002/tji.2020.1347
[55] Turki Jalil, A., Hussain Dilfy, S., Oudah Meza, S., Aravindhan, S., M Kadhim, M., & M Aljeboree, A. (2021). CuO/ZrO2 nanocomposites: facile synthesis, characterization and photocatalytic degradation of tetracycline antibiotic. *Journal of Nanostructures*.
[56] Sarjito, Elveny, M., Jalil, A., Davarpanah, A., Alfakeer, M., Awadh Bahajjaj, A. & Ouladsmane, M. (2021). CFD-based simulation to reduce greenhouse gas emissions from industrial plants. *International Journal of Chemical Reactor Engineering*, (), 20210063. https://doi.org/10.1515/ijcre-2021-0063
[57] Marofi, F., Rahman, H. S., Al-Obaidi, Z. M. J., Jalil, A. T., Abdelbasset, W. K., Suksatan, W., ... & Jarahian, M. (2021). Novel CAR T therapy is a ray of hope in the treatment of seriously ill AML patients. *Stem Cell Research & Therapy*, *12*(1), 1-23. https://doi.org/10.1186/s13287-021-02420-8

[58] Jalil, A. T., Shanshool , M. T. ., Dilfy, S. H. ., Saleh, M. M., & Suleiman, A. A. . (2021). HEMATOLOGICAL AND SEROLOGICAL PARAMETERS FOR DETECTION OF COVID-19. *Journal of Microbiology, Biotechnology and Food Sciences*, e4229. https://doi.org/10.15414/jmbfs.4229
[59] Vakili-Samiani, S., Jalil, A. T., Abdelbasset, W. K., Yumashev, A. V., Karpisheh, V., Jalali, P., ... & Jadidi-Niaragh, F. (2021). Targeting Wee1 kinase as a therapeutic approach in Hematological Malignancies. *DNA repair*, 103203. https://doi.org/10.1016/j.dnarep.2021.103203
[60] NGAFWAN, N., RASYID, H., ABOOD, E. S., ABDELBASSET, W. K., Al-SHAWI, S. G., BOKOV, D., & JALIL, A. T. (2021). Study on novel fluorescent carbon nanomaterials in food analysis. *Food Science and Technology*. https://doi.org/10.1590/fst.37821
[61] Marofi, F., Abdul-Rasheed, O. F., Rahman, H. S., Budi, H. S., Jalil, A. T., Yumashev, A. V., ... & Jarahian, M. (2021). CAR-NK cell in cancer immunotherapy; A promising frontier. *Cancer Science*, *112*(9), 3427. https://doi.org/10.1111/cas.14993
[62] Abosaooda, M., Wajdy, J. M., Hussein, E. A., Jalil, A. T., Kadhim, M. M., Abdullah, M. M., ... & Almashhadani, H. A. (2021). Role of vitamin C in the protection of the gum and implants in the human body: theoretical and experimental studies. *International Journal of Corrosion and Scale Inhibition*, *10*(3), 1213-1229. https://dx.doi.org/10.17675/2305-6894-2021-10-3-22
[63] Jumintono, J., Alkubaisy, S., Yánez Silva, D., Singh, K., Turki Jalil, A., Mutia Syarifah, S., ... & Derkho, M. (2021). Effect of Cystamine on Sperm and Antioxidant Parameters of Ram Semen Stored at 4° C for 50 Hours. *Archives of Razi Institute*, *76*(4), 923-931. https://dx.doi.org/10.22092/ari.2021.355901.1735
[64] Roomi, A. B., Widjaja, G., Savitri, D., Turki Jalil, A., Fakri Mustafa, Y., Thangavelu, L., ... & Aravindhan, S. (2021). SnO2: Au/Carbon Quantum Dots Nanocomposites: Synthesis, Characterization, and Antibacterial Activity. *Journal of Nanostructures*.
[65] Raya, I., Chupradit, S., Kadhim, M. M., Mahmoud, M. Z., Jalil, A. T., Surendar, A., ... & Bochvar, A. N. (2021). Role of Compositional Changes on Thermal, Magnetic and Mechanical Properties of Fe-PC-Based Amorphous Alloys. *Chinese Physics B*. https://doi.org/10.1088/1674-1056/ac3655
[66] Chupradit, S., Jalil, A. T., Enina, Y., Neganov, D. A., Alhassan, M. S., Aravindhan, S., & Davarpanah, A. (2021). Use of Organic and Copper-Based Nanoparticles on the Turbulator Installment in a Shell Tube Heat Exchanger: A CFD-Based Simulation Approach by Using Nanofluids. *Journal of Nanomaterials*. https://doi.org/10.1155/2021/3250058
[67]Raya, I., Chupradit, S., Mustafa, Y., H. Oudaha, K., M. Kadhim, M., Turki Jalil, A., J. Kadhim, A., Mahmudiono, T., Thangavelu, L. (2021). Carboxymethyl Chitosan Nano-Fibers for Controlled Releasing 5-Fluorouracil Anticancer Drug. *Journal of Nanostructures*,